Stability within Jupiter's polar auroral 'Swirl Region' over moderate timescales

Tom S. Stallard[1], John T. Clarke[2], Henrik Melin[1], Steve Miller[3], Jon D. Nichols[1], James O'Donoghue[2], Rosie E. Johnson[1], John E. P. Connerney[4], Takehiko Satoh[5] and Michael Perry[1]

[1]Department of Physics and Astronomy, University of Leicester, University Road, Leicester LE1 7RH, U.K.

[2]Center for Space Physics, University of Boston, 725 Commonwealth Avenue, Boston MA 02215, U.S.A.

[3]Astrophysics Group, Department of Physics and Astronomy, University College London, Gower Street,London WC1E 6BT, U.K.

[4]Goddard Space Flight Center, NASA, Mail Code: 695, Greenbelt , MD 20771

[5]Institute of Space and Astronautical Science, JAXA, Yoshinodai 3-1-1, Chuo-ku, Sagamihara, Kanagawa, 252-5210, Japan

November 26, 2015

Running Head

Stability in Jupiter's polar region

Corresponding author:

Dr. Tom Stallard

Department of Physics and Astronomy

University of Leicester

University Road

Leicester LE1 7RH, U.K.

Email: tss8@leicester.ac.uk

Tel: +44 (0)116 252 3589

Fax: +44 (0)116 252 3555

Abstract

Jupiter's Swirl Region, poleward of the main auroral emission, has been characterised in previous observations as having highly variable auroral emission, changing dramatically across the region on a two-minute timescale, the typical integration time for UV images. This variability has made comparisons with H_3^+ emission difficult. Here, we show that the Swirl region in H_3^+ images is characterised by relatively stable emission, often with an arc of emission on the boundary between the Swirl and Dark regions. Coadding multiple UV images taken over the approximate lifetime of the H_3^+ molecule in the ionosphere, show similar structures to those observed in the H_3^+ images. Our analysis shows that UV auroral morphology within Jupiter's Swirl region is only highly variable on short timescales of ~100s, an intrinsic property of the particle precipitation process, but this variability drops away on timescales of 5-15 minutes. On moderate timescales between 10-100 minutes, the Swirl region is stable, evolving through as yet unknown underlying magnetospheric interactions. This shows that observing the UV aurora over timescales 5-15 minutes resolves clear auroral structures that will help us understand the magnetospheric origin of these features, and that calculating the variability over different timescales, especially >15 minutes, provides a new and important new tool in our understanding of Jupiter's polar aurora.

Introduction

We have a broad understanding of how most of Jupiter's auroral regions are formed, the magnetospheric origin of the currents that drive these aurora, and the auroral morphology which is produced as a result of these currents [Clarke et al., 2004; Badman et al., 2015; Delamere et al., 2014; Grodent, 2015]. However, the source of polar aurorae, in particular emission in the dawn side of this polar region, remains controversial. Ground-based observations have shown that this region is directly associated with the Solar Wind, with ions in this region held at a zero velocity in the inertial frame (Stallard et al., 2003). However, the two leading theories on how the solar wind controls this region require very different interactions with the surrounding magnetosphere. Cowley et al. [2003] evoke an Earth-like Dungey cycle interaction with the Solar Wind, while Delamere and Bagenal [2010] explain the interaction through closed field lines connected to viscous processes with the magnetopause boundary.

Past observations of Jupiter's aurora have been made in numerous wavelength bands, but our understanding of Jupiter's auroral morphology comes broadly from ultraviolet and infrared light. Ultraviolet (UV) aurorae are the result of prompt emission from atomic and molecular hydrogen, as in-falling energetic electrons excite these species, so that the observed UV emission provides a measurement of the instantaneous particle precipitation process, both in morphology and with the brightness of the H_2 Lyman and Werner bands being linearly proportional to the precipitation energy flux. In contrast, infrared observations typically measure emission from the H_3^+ molecule, though IR observations have also been used to study the aurora within H_2 quadrupolar

89 emissions at 2.1 microns [Trafton et al., 1988; Raynaud et al., 2004] and hydrocarbon
90 emissions in the mid-infrared [Caldwell et al., 1983; Kim et al,. 1985]. This H_3^+ is
91 produced by ionising molecular hydrogen in the upper atmosphere then thermalized
92 through collisions with the neutral atmosphere, producing infrared ro-vibrational
93 emission over its ~10 minute lifetime.
94
95 Jupiter's main auroral emission co-rotates with the planet, forming an approximately
96 oval morphology aligned around each magnetic pole, offset from the planet's
97 rotational pole [Connerney et al., 1993; Clarke et al., 1996; Grodent et al., 2008].
98 These main aurorae are driven by the breakdown in corotation within the
99 magnetosphere, when the equatorial plasmasheet, loaded with plasma that originated
100 from the volcanic moon Io, drives currents into the ionosphere [Cowley and Bunce,
101 2001].
102
103 Additional auroral components away from the main emission were initially
104 investigated using ground-based infrared observations of the H_3^+ aurora. These
105 observations also identified an auroral spot and trail directly associated with Io
106 [Connerney et al., 1993]. Other moons have since been shown to have analogous
107 auroral features and the interaction between Jupiter's magnetosphere and its moons
108 that causes these features have been studied in detail in the UV [Clarke et al., 1996;
109 Clarke et al., 2002; Bonfond et al., 2008; Hess et al., 2011]. Poleward of the main
110 emission, Satoh and Connerney [1999] identified broadly stable H_3^+ auroral
111 structures, with a polar region consisting of a 'Ying-Yang' emission, dark in the dawn
112 and bright in the dusk. However, our understanding of the morphology of this region

113 is now much more detailed, as a result of studies of Jupiter's UV auroral morphology
114 [Grodent, 2014; and references therein].
115
116 Figure 1 shows an image of the H_3^+ aurora taken over a CML range of 181-193 at
117 02:35 on the 31 December 2012, constructed from a scan of individual 10s long-slit
118 spectra. The 40" x 0.2" slit of the CRIRES instrument, on ESO's Very Large
119 Telescope, was aligned East-West across the auroral region and scanned through the
120 auroral region over a period of ~15 minutes. The high spectral resolution of the
121 observations (~100,000) results in an auroral image entirely containing only pure H_3^+
122 emission.
123
124 The auroral emission seen in Fig. 1 broadly follows the UV emission described by
125 Grodent et al., [2003]. Both the main emission and Io spot and trail are clearly
126 displayed, though small-scale structures are not easy to distinguish in the IR due to
127 the lower spatial resolution. Poleward of the main emission, the 'Active' region fills
128 the dusk side and has been associated with bright variable emission that forms into
129 flares and arc-like structures, observed to exist over entire sequences of images,
130 suggesting relatively stable structures that last for more than an hour, though this
131 region does see a 2-3 minute periodicity which may be associated with pulsed dayside
132 reconnection [Bonfond et al., 2011]. This region has been shown in past observations
133 to have a H_3^+ brightness between 50-75% of the peak auroral brightness (Stallard et
134 al., 2001). The dawn side of the polar region is split into two regions. The 'Dark'
135 region is a crescent shaped region adjacent to the poleward edge of the dawnside main
136 auroral emission. In the UV, this region is almost devoid of auroral emission, the
137 order of only a few tens of kR above the background level. Past IR ground-based

138 observations of this region have proven difficult, as it is narrow, and turbulence in the
139 Earth's atmosphere usually blends this region with the surrounding main oval and
140 Swirl regions. In Figure 1, where the observing conditions are particularly clear, this
141 region is clearly visible, and has an emission ~25% of the peak auroral brightness.
142 Poleward of this, the 'Swirl' region, in UV emission, is a region of faint patchy
143 emission features that occasionally form swirls. Emission in this region appears to be
144 transitory, with emission features changing from image to image, suggesting the
145 features occur with a cadence of ~100s [Grodent et al., 2003]. Past observations have
146 suggested the presence of arc-like features in this region, both following the main
147 auroral emission [Pallier and Prangé, 2001] and producing trans-polar arcs [Nichols et
148 al., 2009], but such observations have remained controversial due to the essentially
149 transient nature of the emission in this region. Past H_3^+ observations have shown that
150 this region appears much less variable in the infrared, producing a general brightening
151 of ~50% the peak auroral brightness (Stallard et al., 2001).
152
153 Despite differences in production, the broad distribution of the H_3^+ and UV aurora
154 have previously been shown to be similar, particularly on the main auroral emission
155 and within the aurora associated with moon interactions, with the major differences
156 most likely the result of changing temperature driving variability in the H_3^+ emission
157 [Clarke et al., 2004, Radioti et al., 2013]. The Active region has also been shown to
158 have broadly similar in morphology in both wavelengths [Clarke et al., 2004; Radioti
159 et al., 2013]. However, the Swirl region shows significant differences in the
160 instantaneous emission in the two wavelengths. The differences seen are dominated
161 by the high variability seen within the UV Swirl aurora, making any comparison with
162 the more long-lived H_3^+ emission difficult.

In this paper, we will identify the typical H_3^+ emission structure seen within the polar region. We will then look at the UV emission over an extended timescale, removing any short-term variability, so that the emission can be observed under similar conditions as H_3^+ emission and a direct, like-for-like, comparison of morphology can be made.

H_3^+ infrared images

Jupiter's H_3^+ aurorae have been observed in detail over an extended period of time, including extensive observations between 1995-2000 by J. Connerney and T. Satoh using the NSFCam instrument on the NASA Infrared Telescope Facility (IRTF) [Shure et al., 1994]. The data was reduced using the methodology laid out in Satoh and Connerney [1999], with individual images undergoing sky subtraction, bad-pixel removal and image flattening. These individual images are then cross-correlated, shifted, and added together to reconstruct one final image, combining 6 sets of 20 coadded 1s integrations, for a total integration time of 120s. Each image has a pixel scale of 0.148". For this paper, we have chosen those observing nights with clear observing conditions and where the northern auroral oval was observed with at least 5 different central meridian longitudes (CMLs) in 10-degree steps, between CMLs of 140 and 210. These constraints resulted in the seven separate nights and a total of 45 images, shown in Figure 2. These images are taken using two very narrow (spectral resolution 200) filters, centered on either 3.4265 micron or 3.542 micron.

These images clearly show the Active, Swirl and Dark regions are common within all the images, and are thus common features of both the UV and H_3^+ aurora. On long timescales (while observing from night to night), the polar region of Jupiter appears to change significantly in morphology and relative brightness. At times the Active region is broadly infilled with emission typically ~75% the peak emission brightness (29jun95, 27jul98 and Fig 1: 31dec12), while at other times it is dominated by bright arcs and spots that are as bright as the main oval (23sep99, 11oct99 and 19dec00), similar to those seen in the UV emission, and at times relatively little emission is seen in this region, with emission as dark as only ~40% peak emission brightness (08jul96). The Swirl region seems to have comparable variability, sometimes appearing to be infilled with emission typically ~50% peak emission brightness (27jul98 and Fig 1: 31dec12), often having a crescent arc of emission inside the main auroral emission that is between 50-80% peak emission brightness (29jun95, 23sep99 and 19dec00), which appears to be co-located with the boundary between the Dark Region and Swirl region, and sometimes appearing to have little emission, as low as only ~30% peak emission brightness (08jul96 and 07aug97). Even on those nights when little emission is seen in the Swirl region, the emission in this region is notably brighter than the emission in the Dark region, which appears to have typical a emission brightness of ~25% peak emission brightness.

Three additional regions are repeatedly identifiable within the H_3^+ auroral emission. Firstly, broad region of limb-brightening that extends down the dusk limb. This brightening is likely to be caused by dayside H3+ rotating over the limb, allowing an increased line-of-sight enhancement as it move above the underlying dark disk of Jupiter. In contrast with this is the generally dark dawn limb, which sees the nightside

212 ionosphere rotating into view. Generally, this nightside ionosphere has no H_3^+ away
213 from the auroral region (Stallard et al,. 2015), and so, as this ionosphere empty of H_3^+
214 rotates onto the dayside, there is no emitting H_3^+ to be limb-brightened. However, a
215 second feature seen within these images, a weak dawn limb-brightened emission, is
216 sometimes observed. This appears as a narrow arc with a brightness ~25% the peak
217 emission brightness, at magnetic latitudes that approximately map to the Io torus. This
218 occurs on multiple nights when the Io spot is clearly located near noon (07aug97,
219 19dec00 and marked as (L) on Fig. 1: 31dec12). This brightening is not matched by a
220 localised dusk enhancement, suggesting that it is associated with more than just the
221 limb-brightening of the Io trail, which would produce a stronger dusk emission when
222 the Io spot itself is near noon. Thirdly, a region of auroral darkening also appears
223 close to the magnetic pole of the planet, in between the Swirl and Active regions. This
224 region has a similar brightness as the Dark region, with typical emission ~25% the
225 peak emission brightness. At times, this appears as a narrow dark channel that appears
226 to follow the inner edge of the Active region (in particular 11oct99; marked as (P) in
227 Fig. 1: 31dec12), but at other times it is a broader dark region centered on the
228 magnetic pole (29jul95, 27jul98 and 19dec00). This may be a region of reduced
229 particle precipitation, but equally might be caused by a lack of heating across the
230 magnetic pole, perhaps indicating that the ionospheric currents that drive Joule
231 Heating are minimised here.
232
233 Other previously identified UV auroral features can also be seen within these images,
234 such as an apparent trans-polar arc (08jul96) similar to that identified by Nichols et al.
235 [2009a] and an extended region of isolated emission equatorward of the main oval

236 (07aug97) like those Bonfond et al. [2012] has previously identified and attributed to
237 the injection of depleted flux tubes.
238
239 However, while there is significant variability on longer timescales, many of these
240 different broad-scale structures in the polar region are stable over the timescales of the
241 observations on each individual night, so that they are seen approximately rotating
242 with the planet between CMLs of 140 and 210, over ~90 minutes (as Jupiter rotates
243 by ~0.6 degrees per minute). In most cases, these structures evolve to some extent
244 over this timescale, and some change significantly on timescales as short as only ~30
245 minutes (e.g. the Active Region on 23sep99). However, most notably, none of the
246 aurora has significant variations on timescales <30 minutes, most notably in the Swirl
247 region where the UV aurora shows significant short-term variability.
248
249 This short-term temporal stability in the H_3^+ aurora results from the extended ~10-15
250 minute lifetime of the molecule in Jupiter's ionosphere [Achilleos et al., 1998; Tao et
251 al., 2011], so that short-term bursts of particle precipitation provide only a partial
252 contribution to the total ionisation of H_3^+ over a 10-minute period. If particle
253 precipitation in the Swirl region resulted in truly random UV emission patches, the
254 H_3^+ emission in this region would emit as a uniform dim glow, as random
255 precipitation, varying over ~100s, would uniformly ionise the entire Swirl region over
256 the 10 minute lifetime of H_3^+. The presence of stable arc structures, concentrated on
257 the boundary between the Swirl and Dark regions in the H_3^+ emission must, thus,
258 result from either one or from a combination of both of the following processes:
259

1) A uniform H_3^+ density across the region is preferentially heated along the boundary between the Dark and Swirl regions, resulting in a thermally enhanced H_3^+ emission in this region. This heating may be the result of the significant sub-rotation observed in this region [Stallard et al., 2001; 2003], which dominates heating in the auroral region though joule heating [Melin et al., 2006].
2) The H_3^+ density is enhanced by increased ionisation along this region, as a result of currents driving particle precipitation along the Dark and Swirl region boundary. This second possibility would require that similar structures also exist in the UV emission, with these features obscured on the timescale of individual images by an apparently random process inherent to particle precipitation process.

H and H_2 UV images

If the dawn structures observed in the H_3^+ emission are the result of particle precipitation, they will also occur in the UV aurora, and will become apparent when observed over similar time-scales as the H_3^+ lifetime. In order to test this, we must emulate the H_3^+ lifetime within the UV emission by temporally averaging UV emission over 12 minutes, emulating the H_3^+ ~10-15 minute lifetime. For such emulation, we must combine multiple UV images, each taken within the 12 minute period. Unfortunately, early observations of the UV aurora, including the simultaneous data from 2000 presented in Clarke et al. [2004] and Radioti et al. [2013], were taken further apart in time.

Instead, we use images of Jupiter's northern FUV auroral emission obtained by the solar blind channel (SBC) of the Advanced Camera for Surveys (ACS) on board HST over January-June 2007, as described in detail within Clarke et al. [2009]. As described in that paper, the Solar Blind Camera (SBC) on ACS has a wavelength band pass of 115–170 nm including the H_2 Lyman bands, Werner bands, and the H Ly-α line. For clear images, using the F115 filter, assuming an auroral spectrum, the assumed conversion factor from counts per second per pixel to kRayleigh is 0.0021. This study also uses filtered images taken in the same HST orbit with the ACS filter F125LP (>125 nm), using a flux conversion factor to kRayleigh of 0.00028 counts per second per pixel. The images within each set of observation used were taken in bursts, with multiple images taken within a single orbit, providing the time resolution needed to emulate the H_3^+ images. In order to produce a useful comparison, we have limited our investigation to auroral images that are suitably similar: we have used only images that have a 100s integration time, that observe the northern hemisphere, and that include at least one image with a CML between 170-190 (so that we have a clear view of the northern aurora). All the sets of observation we have utilised have the same observing pattern: five images using the F125 filter, eight images using the F115 filter, then a final five using the F125 filter, providing total of eighteen images on each day. The F115 filter is open, including the bright H Ly-α emission at 121.6nm, while the F125 filter excludes this emission below 125nm, and so is dominated by H_2 auroral emission. For the purposes of this study, we have assumed that the auroral emission within these two filters is identical; we will test this assumption later in the paper.

The UV images were processed using a pipeline that has been extensively discussed previously [see, e.g., Clarke et al., 2009; Nichols et al, 2009b], background reflected sunlight being modelled and removed and with units converted from counts to kR. Figure 3 shows a sequence of images of Jupiter's UV aurora taken on May 16, 2007 with individual exposures of 100s, and a total observation time of ten minutes.

These images have then been combined; however, simply coadding these images would result in significant smearing of the emission in longitude, as the planet rotates by 6 degrees during this period. In order to account for the longitude variation while adding these images, the images were projected onto a planetocentric latitude-longitude grid assuming an emission altitude of 240 km [see Grodent et al., 2003b for details]. Once mapped in latitude and longitude, we averaged all the resultant maps of emission, then re-projected the combined emission map back into the viewing angle seen from Earth. This results in a 12-minute time-averaged UV image, shown as the bottom panel in Figure 3, free of the smearing effect of the planets rotation, analogous to the H_3^+ images shown in Figure 2.

The result of this combination of images is that polar features seen in this region appear to be much more clearly resolved. Although the peak brightness of auroral features in the polar region is reduced, the region as a whole is filled with continuous emission of moderate brightness (~100kR). The Dark Region is very well defined and may have some low-level emission associated with it (~40kR). Both the Active and Swirl regions have arc-like features crossing them, most notably an arc that appears to follow the boundary between the Dark and Swirl regions (which peaks at ~150kR).

In Figure 4, we have repeated this coadding of individual images across twelve sequences of images, each covering a total of ~45 minutes, from the north auroral regions on various days within 2007. What is immediately apparent from these images is that for each day, the three coadded image appear very similar. This means that the morphology of Jupiter's UV polar emission appears to be far more stable when observed over moderate timescales. However, on longer timescales, between days, the polar auroral structure varies significantly in morphology.

On some nights, a bright arc of emission can be seen between the Dark and Swirl regions, with bright spots located along the edge of this arc each day. On some days, this arc is discrete (27feb07, 11may07, 16may07, 18may07, 27may07, 03jun07), while at other times it appears far more diffuse (04mar07, 05mar07, 07jun07), and often includes brighter sub-structures, such as spots and arcs (e.g. 03jun07). On other nights there is no obvious arc of emission between the Dark and Swirl regions; this appears to occur mostly when the Dark region is particularly dark (<10kR; 12may07, 13may07, 17may07, 23may07, 31may07, 10jun07), although there are examples where that is not the case (26feb07, 29may07, 08jun07). When this happens, the boundary between these regions appears to be more poleward, and in most cases the swirl region also has significant bright spots within it (with the clear exception of 08jun07, and possibly 23may07). Although the boundary is sometimes a gradual transition in brightness (10jun07), in most cases the boundary itself has fragmented arcs or dots of emission along it (12may07, 13may07, 17may07, 23may07) and in one case has a thin faint arc close to the boundary (31may07). The apparent anti-correlation between the occurrence of bright high-latitude spots of emission and a bright arc of emission on the boundary between the Dark and Swirl regions may be

358 indicative of changing magnetospheric conditions, though the wide variety of
359 morphologies observed shows that any correlation is complex, and needs a more
360 detailed study to fully understand.
361
362 The Active region clearly varies dramatically on different days, with many of
363 previously identified features (Grodent et al., 2003), such as bright emission close to
364 the main oval (04mar07, 07jun07), multiple arcs across the region (05mar07,
365 11may07, 27may07) or bright spots between the Active and Swirl regions (26feb07,
366 27feb07, 17may07). Arc-like structures appear to be relatively stable on moderate
367 timescales, but the intensity of bright spots changes significantly over these moderate
368 timecales.
369
370 We can also look for evidence of those features identified in our H_3^+ images. The
371 region of polar darkening, marked as (P) on Fig. 1, is not readily apparent within the
372 UV emission, even on moderate timescales. There is one day where the region around
373 the magnetic pole appears to be darker than the Dark region (11may07), though this
374 may be due to poor background subtraction on this day. This lack of a clear boundary
375 suggests that the H3+ density in this region is also relatively smooth, and so is a
376 strong indicator that the difference in H3+ emission brightness results from a
377 significant change in the thermospheric temperature in this region, most likely
378 because of the significant ion winds within the Swirl region driving strong Joule
379 heating in that region. There is more evidence for an enhancement in the Limb
380 brightening, marked as (L) on Fig. 1, within the UV emission. At least two nights
381 show a dawn limb brightening at times when the Io spot is clearly visible on the body
382 of the planet (26feb07, 04mar07). The scale of the enhancement (~25% the peak

383 brightness) is very similar to the enhancement observed in H_3^+ brightness, suggesting
384 that this feature may be caused by enhanced across the precipitation across the dawn
385 terminator.
386
387 Having shown that summing individual UV images over a period equivalent to the
388 lifetime of H_3^+ results in images that, like H_3^+ images, produce relatively stable broad-
389 scale polar structures. We will now attempt to quantify both the timescales of
390 variability previously observed in the polar region, and whether longer-timescale
391 variability is also seen.
392
393 Figure 5 shows Jupiter's aurora from May 16, 2007 in the top frame, the same aurora
394 shown in Fig. 3, but here show the integrated intensity from all 18 images within the
395 sequence taken on that day. For clarity, we have also labelled the emission features
396 described in Fig. 1. Unlike that auroral image, on the May 16, the Io spot is located
397 on the midnight side, and so the dawn enhancement may be a combination of both the
398 line-of-sight enhanced Io tail and/or an additional dawn limb component.
399
400 In order to understand the variability seen across the auroral region, we have
401 calculated the standard deviations in intensity within each mapped latitude-longitude
402 grid position, across the individual observations that were combined to make this
403 image. This produces a map of the standard deviations across the sub-images with
404 time, shown in the middle panel of Fig. 5, effectively showing the auroral variability
405 across the total period of observation; this variability is measured between individual
406 images, and so has effective cadence of 100s.
407

What is immediately apparent is that while past discussions of variability have highlighted the variability within the dawn polar region (e.g. Grodent et al., 2003a), the absolute variability across the whole region is significantly less than that seen on the main auroral emission. The bright auroral arc seen between the Swirl and Dark regions is one polar region where variability is comparable that seen in the main auroral emission. The brightness variation in this region has previously been shown to match with changes in the main oval brightness, and has tentatively been associated with changes in plasma circulation processes within Jupiter's magnetosphere, indirectly controlled by changes in Io volcanism (Kimura et al., 2015). In our measurements, we also show significant variability in the Active region, including a localised region of significant variation in the dusk-midnight sector.

However, while this figure reveals the regions of absolute variability, it fails to highlight the variations in the Swirl region. The reason variability in this region has been highlighted in the past is that the magnitude of variability is significant compared with the absolute brightness of the emission.

In the bottom panel of Fig. 5, in order to reveal this variability, we have divided the standard deviations by mean auroral brightness, resulting in a map of standard deviations as a percentage of auroral brightness, scaled between 0-100%. Most notable here is the non-aurora region, where true noise within the image is revealed as a broad region where the scaled standard deviations are often >100%, where the variation is significantly larger than the averaged intensity. However, within the auroral region, where the signal-to-noise is relatively low, both the Swirl and Dark regions are revealed as the parts of the polar aurora with the largest scaled standard

433 deviations. The relative variability associated with the main auroral emission is now
434 very small, while bright polar auroral features have a similar level of scaled variability
435 as the rest of the polar region.
436
437 This variability across individual images is the same variation described in past papers
438 (e.g. Grodent et al., 2003a). In order to better understand how this variability changes
439 across different timescales, we will repeat the calculation of the scaled standard
440 deviations, but using a combination of multiples of individual observations. To
441 calculate this, we bin the individual images into five timescale sets, covering the
442 binning of 2, 3, 4, 6 and 9 images. Each of these sets is produced from the averaging
443 of individual images, with each averaged image containing unique images: when
444 binning 2 images, we average images 1+2, then 3+4, then 5+6, and so on; when
445 binning 3 images, we average images 1+2+3, then 4+5+6, and so on; finally, when
446 binning 9 images, we average all images between 1 and 9 and then all images between
447 10 and 18. We then measure the mean standard deviations across each of these sets of
448 images, and scale this against the mean auroral brightness across the entire time
449 period, in the same way as described above for Fig. 5. Each individual image takes
450 100s to integrate, with an additional 40s between each observation. This results in six
451 timesteps: 1 minute 40 seconds; 4 minutes; 6 minutes 20 seconds; 8 minutes 40
452 seconds; 13 minutes 20 seconds; and 20 minutes and 20 seconds.
453
454 The resultant scaled standard deviations are shown in the left column of Fig. 6, for
455 each of the different time steps. When integrating over longer and longer periods, the
456 characteristics of the observed variability changes. In all time steps, the noise away
457 from the auroral region dominates, with typical scaled standard deviations above

458 100%, though this reduces at longer integration times. Within the auroral region, the
459 Swirl region dominates the scaled standard deviations from individual image to image
460 (top-left, and Fig. 5), with scaled standard deviations at ~35% emission brightness.
461 However, when comparing the scaled standard deviations from images averaged over
462 twenty minutes (bottom-left), the variability in this region has been reduced
463 significantly. Regions near noon and midnight have scaled standard deviations of
464 ~25%, but the core part of the swirl region has scaled standard deviations as low as
465 ~5-10%. Other parts of the aurora maintain their variability over much longer
466 timescales, most notably the localised variability in the dusk-midnight sector, and the
467 arc near noon, with scaled standard deviations ~30-40% emission brightness.
468
469 In order to better understand the timescales at which the Swirl region transitions from
470 highly variable to more stable, we must analyse the differences in variability between
471 the time steps. In the middle column of Fig. 6 we show how variability decreases as
472 additional observations are added together. This is produced by dividing the scaled
473 standard deviations measured across individual files (top-left) by the scaled standard
474 deviations for each subsequent set of time steps (left column). Each image shows a
475 percentage change in variability between 30-300% (with red showing variability at
476 30% the original variability and blue at 300% the original variability). As such, the
477 first resultant difference map, the top middle panel of Fig. 6, shows the difference
478 between the 1m 40s and 4m time steps.
479
480 The most obvious result from this analysis is that the total variability within the polar
481 region reduces to a greater and greater degree with increasing timestep. The
482 difference in variability between the two most extreme time steps, 1m 40s (100s) and

20m 20s (middle-bottom) sees the variability in the Swirl region reduced to 25-33% of the variability seen in individual images. The variability within the brighter auroral emission does not change significantly between these time steps.

To better understand the timescales of variability, we can also analyse the changes in variability between sequential time steps. In the right column of Fig. 6 we divide the variability of a time step by the immediately subsequent time step, so that the final panel of Fig. 6, bottom right, consists of the variability within the 13m 20s time step divided by the variability within the 20m 20s time step. Here, each image shows a percentage change in variability between 60-140% (with red showing variability at 60% the variability of the shorter time step and blue at 140% the shorter time step).

These plots show that for timescales of less than 6m 20s, variability always reduces, across the entire auroral region, as the time step increases. This suggests that the entire auroral region has significant auroral variability over a ~0-5 minute time period that is smoothed by combining the data over the length of this time period. However, between 6m 20s and 13m 20s, while the majority of the Swirl and Dark region see continued reduction in variability, the Active region and some regions of bright emission in the Swirl region now see increasing variability (shown in blue). This suggests that these regions have variations in the 5-15 minute timescale, which matches well with past observations of these regions (e.g. Grodent et al., 2003). The final time step, between 13m 20s and 20m 20s, sees a dramatic change in the overall variability, with significant increases in variability within the majority of bright regions. This variation is greatest in the noon sector of the Swirl region, suggesting this region is significantly more variable at moderate timescales of >15 minutes, with

508 an increase of ~140%. The main auroral emission also sees an increase in variability
509 in at this longest time step, getting ~120% more variable. This correlates well with the
510 variability seen within Fig. 1, where the H_3^+ images have broadly similar structures,
511 but the relative brightness of these structures appears to change over a 1-2 hour
512 period. This variability is, in turn, likely to be the start of longer timescale variations
513 that ultimately lead to the significantly different auroral configuration on sequential
514 days of observation, as can be seen in Figs. 4 and 7.
515
516 Figure 6 has shown us that smoothing the data temporally can significantly reduce
517 short-term variability, resulting in a greatly reduced variation in the Dark and Swirl
518 regions of the polar aurora. However, at timescales ~>15 minutes, variability begins
519 to increase again. In Figs. 4-6, we have only analysed the variation seen within a
520 single day of observation.
521
522 In Figure 7, we show the average emission across the entire period of each
523 observation, effectively the average of each set of three images in Fig. 4. This again
524 reveals the broad structures discussed in Fig. 4. Below each of these images, we also
525 show the absolute standard deviations using a time step of 13m 20s, effectively the
526 average standard deviations across the three images shown in Fig. 4. This shows that
527 the extent of polar variability changes significantly across the set of auroral images
528 studied here. In all these images, the absolute variability is largest in the brightest
529 regions. The Active region appears to have a large variation in the majority of the
530 images, though on a few days (13may07, 18may07, 03jun07) this region varies less
531 than the Swirl region. The Swirl region appears to have periods of low variability
532 (04mar07, 11may07, 12may07, 08jun07, 10jun07), periods where variability is low,

except in the noon bright arc region (26feb07, 16may07, 23may07), periods when there appears to be an oval of variability surrounding the Swirl region (27may07, 29may07, 03jun07) and times when the entire polar region is highly variable (27feb07, 18may07).

Such dynamic variability makes it difficult to make conclusions about the drivers of this variability from this relatively small number of auroral observations investigated here, but it seems to indicate that there are multiple sources of variability within the polar region, that often correlate with emission brightness, but can act with significant independence from it.

So far, we have assumed that the measured auroral emission from the two different HST filters (F115 and F125) is the same, despite the F125 filter excluding the dominant H ly-α emission at 121.6nm. In Figure 8 we test this assumption by assessing and comparing the average emission brightness and variability measured in these two separate filters. We have taken the measured emission for combined orbit of observation, each of which consists of five F125 observations, eight F115 observations, then five F125 observations. Firstly we calculated the average emission measured within each of these two filters across all eighteen days we have used in this study. The observed emission within the two filters, shown in the left column of Figure 8, is very similar when compared by-eye, with the most notable differences falling within the Active region, where the open F115 filter appears to show multiple arcs inside the main oval, while the F125 filter appears to have more spotted structure. There are no notable differences within the Dark and Swirl regions, though these regions are significantly darker, and so differences might be difficult to observe.

In order to properly emission within the two filters, we calculate the absolute difference in brightness across the two filters, and scale this against the average brightness of both filters. This difference in auroral emission is largest close the main auroral oval, where the differences measured are ~20% of the auroral brightness. Although some parts of the active region have differences significantly higher than this, these spots are caused by individual events that would produce significant differences irrespective of the filter used. Interestingly, a section of the Dark region close to Dawn shows an emission change with filter of >10%, which comes because this region is consistently darker in F125 than in F115. However, the emission observed in the Swirl region differs very little between the two filters, with the two filters differing by <5% in this region.

In order to assess the change in variability between the two filters, we have calculated the variability at the shortest timescale, observing the difference in emission on between subsequent images, ignoring the differences between images when the filter changes. We then take the average of these differences within each filter, as is shown in the right column of Figure 8. The variability seen within the two filters is not notably different across the majority of the auroral region, though it does appear somewhat higher in filter F125, in particular within the Active region, where bright auroral spots appear to change significantly. This increased variability is most likely caused by bursts of particle precipitation which penetrate below the homopause for a short time (<100s), resulting in hydrocarbons absorption of the H2 auroral emission, enhancing the changes in brightness observed from one image to the next. These differences are highlighted in the bottom image in the right column of Figure 8, which

583 directly shows the differences in variability between the two filters. Again, the largest
584 differences are seen in the Active region, but the Swirl region is also somewhat more
585 variable in F125 than in F115.
586
587 These filter dependent differences in variability will have an effect upon the variation
588 values presented earlier in the paper. However, this effect is minimised at shorter
589 time steps, where most of the calculated variability will occur in images from the
590 same filter, and at the longest 20m 20s time step, where the 5, 8, 5 observing pattern
591 means that any changes in the observed variability will be equally balanced between
592 the two timesteps. It will be maximised in the 13m 20s, where the three sets of
593 images used to calculate variability fall close in timing to the change in filter within
594 the observations. However, Figure 6 appears to show a clean progression of
595 variability from the shorter to longer timesteps, with no obvious increase in variability
596 at 13m 20s, suggesting that the effect of changing filter is minimal when compared to
597 the true variability within the auroral features.

598 ## Conclusion

599

600 In conclusion, by producing UV images effectively integrated over a twelve minute
601 period, we show similar polar structures to those seen in H_3^+ emission, where the
602 lifetime of H_3^+ naturally enforces a ~10-15 minute temporal smoothing to the particle
603 precipitation processes. This shows, for the first time, that auroral morphology within
604 Jupiter's Swirl region exhibits broad auroral features driven by and indicative of
605 large-scale magnetospheric interactions. On short timescales of ~100s, the particle
606 precipitation and resultant UV emission are highly variable, suggesting that the
607 particle precipitation process has an intrinsic variability associated with it. This

608 variability falls away on timescales between 5-15 minutes, resulting in a relatively
609 stable Dark and Swirl regions. On timescales >15 minutes, some brightness
610 variability is seen, but images of the H_3^+ aurora show that broad structures observed
611 within the Swirl region are present for at least 100 minutes. On some days, significant
612 variability remains in the Swirl region at moderate timescales, though in all cases,
613 variability is reduced between 2 and 20 minutes. This indicates that the short-term
614 variability observed and commented on in past papers within the Swirl region
615 dominates only on the relatively short term timescales of individual images, and on
616 longer timescales structures that are indicative of the underlying magnetospheric
617 interaction are observed across the polar auroral region.
618
619 One dominant feature regularly observed in H_3^+ emission, and apparent with the UV
620 emission investigated here, is a bright arc of emission on the boundary between the
621 Dark and Swirl regions. Importantly, this confirms the existence of polar auroral arcs
622 seen by Pallier and Prangé [2001], though further investigation is required to properly
623 assess their conclusion that these arcs extend into the Active region. If the Swirl
624 region represents the region of open field lines, as has been suggested using velocity
625 measurements [Cowley et al., 2003; Stallard et al., 2003], this arc of emission could
626 be analogous to the main auroral emission produced at Saturn and Earth. Comparison
627 of the size of the Swirl region would then also provide a direct measure of location of
628 open flux, which, when mapped out along magnetic field lines, could provide
629 important constraints to our understanding of the outer magnetosphere, an improved
630 version of the modelling performed by Vogt et al. [2011] who used the location of the
631 main auroral oval to produce an estimate of the region of open flux. If, however, the
632 dawn polar region maps to the flanks of the magnetosphere [Delamere and Bagenal,

633 2010], this emission provides important clues as to how such a process occurs. The
634 brightness of this feature may be significantly enhanced in the H_3^+ emission as a result
635 of additional heating in this region, the result of the expected joule heating associated
636 with strong sub-rotation in the dawn polar region.
637
638 Future investigation of the polar region of Jupiter should examine the changes in this
639 underlying structure (in either UV or IR emission) with changing conditions in the
640 surrounding magnetosphere and solar wind, in order to identify the underlying
641 influences on what has been previously considered a highly variable polar region, and
642 utilising the wider sets of auroral observations not investigated in this study,
643 potentially revealing further information about both the magnetospheric conditions
644 and the conditions within Jupiter's upper atmosphere. Such studies should also
645 investigate the observed variability on different timescales, which this study shows is
646 a useful tool that reveals new details within the aurora. In addition, given the
647 similarities between UV and IR aurora over comparative timescales, any future
648 investigation of the differences between these aurora will need to include the effects
649 of temporal smearing within any UV observations used for comparison.
650
651
652
653
654
655
656
657

658

659

660

661

662

663

664

665

666

667

668

669

Figures

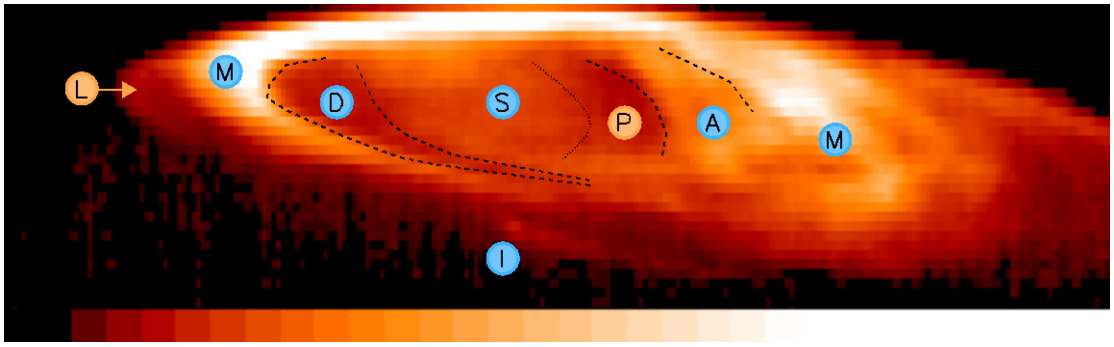

Figure 1: Jupiter's H_3^+ northern auroral morphology. This image, started at 02:35 on the 31 December 2012 and constructed from a scan of individual 10s long-slit spectra, was collated over ~15 minutes, with each vertical pixel representing emission from a single spectrum. It shows the northern auroral emission from the H_3^+ ν_2 $Q(1,0^-)$ spectral line at Jupiter, at a CML of 181-193. The major UV auroral features are identified (M: Main emission, D: Dark region, S: Swirl region, A: Active region and I: Io spot and trail; Grodent et al., 2003), along with two regions commonly seen within H_3^+ images (L: dawn Limb brightening, P: Polar darkening). A linearly increasing scale is presented at the bottom, ranging from 0-1.52 Wm^{-2} $\mu m^{-1} str^{-1}$.

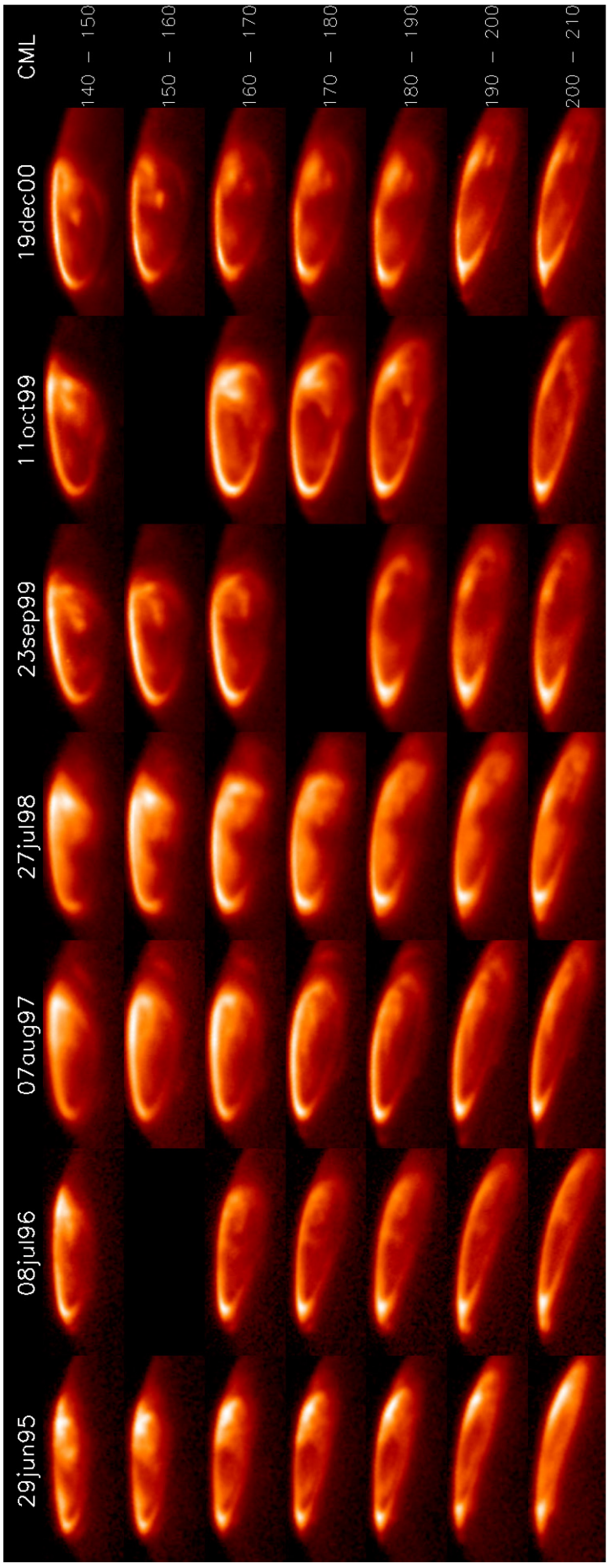
CML
19dec00
11oct99
23sep99
27jul98
07aug97
08jul96
29jun95
140 – 150
150 – 160
160 – 170
170 – 180
180 – 190
190 – 200
200 – 210

684

685

686 Figure 2: Jupiter's H_3^+ northern auroral variability. These images, taken over a period
687 of five years (left to right) show the changes in morphology with time and central
688 meridian longitude (~16 minute steps, ~10 degree steps; top to bottom). While the
689 main auroral emission is relatively stable on long timescales, the region poleward of
690 this is highly variable, with significant differences in both the Swirl and Active
691 regions from year to year. However, on any particular day, the emission structures
692 seen within the pole are consistent across the period of observation, with changes
693 occurring slowly over several images (with timescales >30 minutes).

694

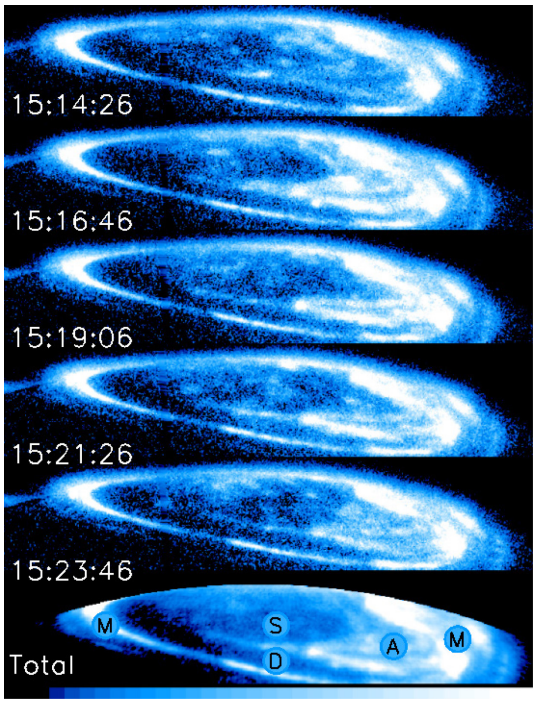

695

696 Figure 3: Individual images of Jupiter's northern auroral UV aurora on 16 May 2007,
697 and the co-added product of these images. Each image integrates for 100s, and the
698 resultant morphology is very similar on the main auroral emission, but shows
699 significant changes in the polar regions. The intensity has been scaled to highlight
700 polar emission. Each image is polar projected and rotated to the same CML of the

final frame, before co-adding, allowing the images to be coadded temporally, without spatial smearing. This image is also shown in Figure 4, as the first image in the 16may07 sequence. Also note the lack of emission above the limb, lost through the polar projection process. The intensity stretch used for the images is shown with the linear scale at the bottom, ranging between 0-200 kR.

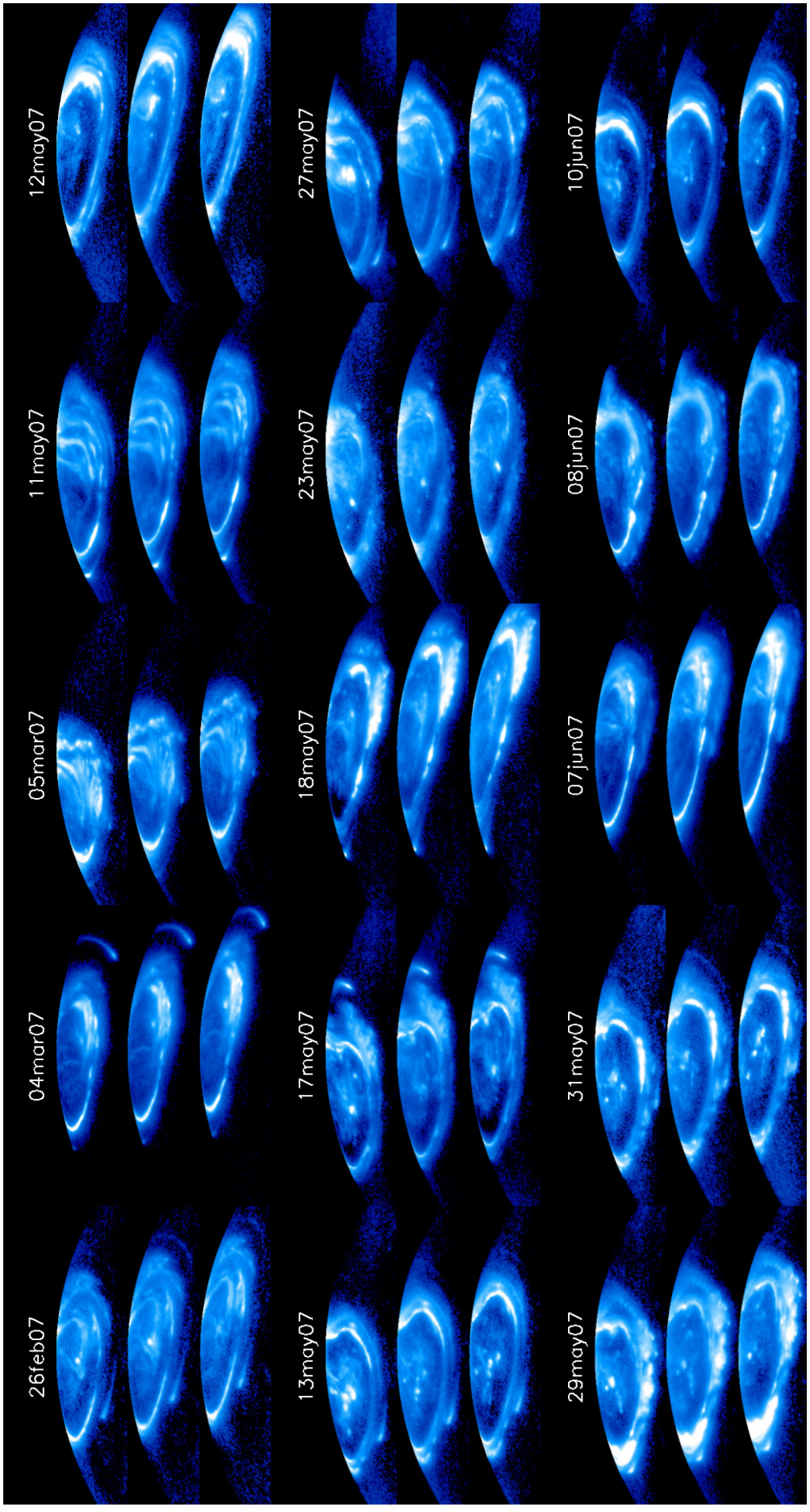
26feb07
04mar07
05mar07
11may07
12may07
13may07
17may07
18may07
23may07
27may07
29may07
31may07
07jun07
08jun07
10jun07

707

Figure 4: Eighteen sequences of coadded images for the auroral region, from various observations across 2007. Each of these coadded images is made up of multiple individual images taken over a total of ~12 minutes, so that the whole sequence of three coadded images covers ~45 minutes. Emission intensity is scaled to highlight polar emission, with values ranging between 1/20 and 5 times the mean value within the auroral region of each image, displayed with a gamma correction of 0.3. This clearly shows that significant stable structures can be identified in both dawn and dusk regions on timescales similar to those seen in the H_3^+ emission.

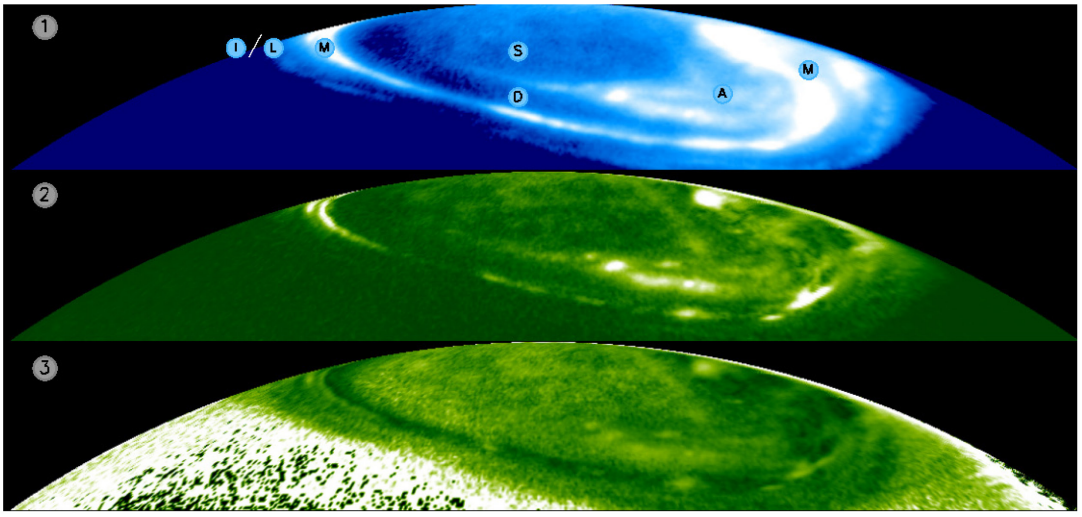

Figure 5: Jupiter's integrated auroral intensity from all 18 images from 16 May 2007(1; blue), is shown same labelled emission features as described in Fig.1. Here, the emission ranges between 20-200 kR, and has been gamma corrected with the equivalent of a fifth-order-root of the values (a gamma correction of 0.2) – this

723 reveals the polar auroral features more clearly. In the middle (2; green), we show the
724 average standard deviations within the 18 individual images across this entire
725 sequence, scaled linearly between 2.2-8.9 kR (representing a variance of 5 – 80 kR).
726 At the bottom (3; green), we show the average standard deviations as a percentage of
727 auroral brightness, scaled between 0-100%.
728

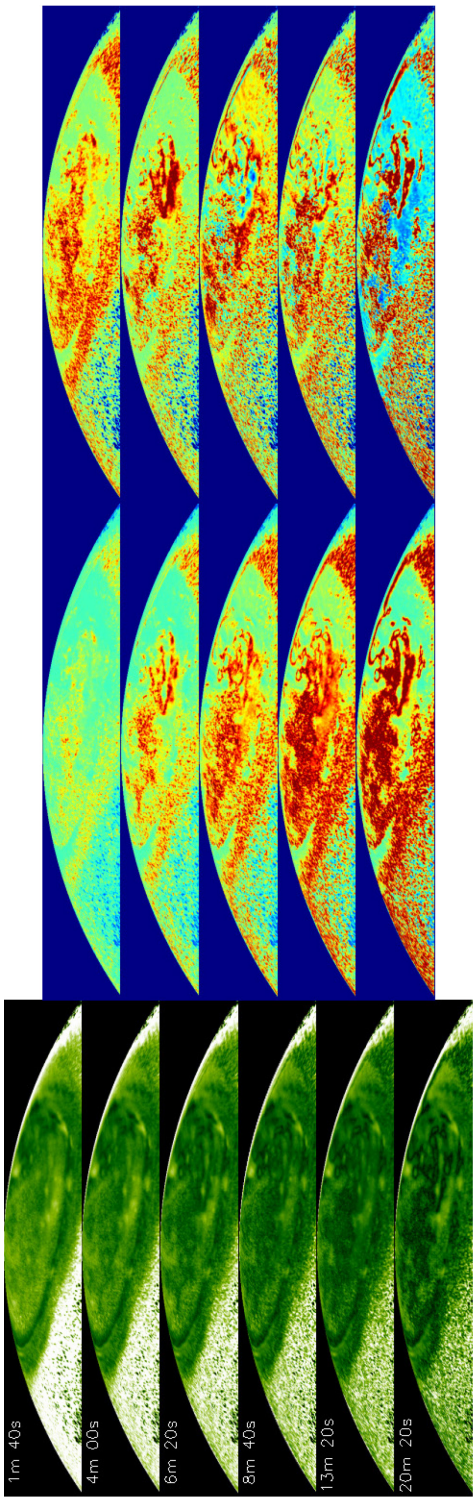

Figure 6: In the left column, we show the average standard deviations as a percentage of auroral brightness (shown in green), a measure of the auroral variability across six different time steps between 1m 40s and 20m 20s, scaled between 0-100%. In the central column, we show the percentage difference between the shortest time step and the five longer time steps, scaled between 30-300%, with blue showing increased

variability and red showing decreased variability. In the right column, we show the percentage difference between each sequential time step, scaled between 60-140%, again with blue showing increased variability and red decreased variability.

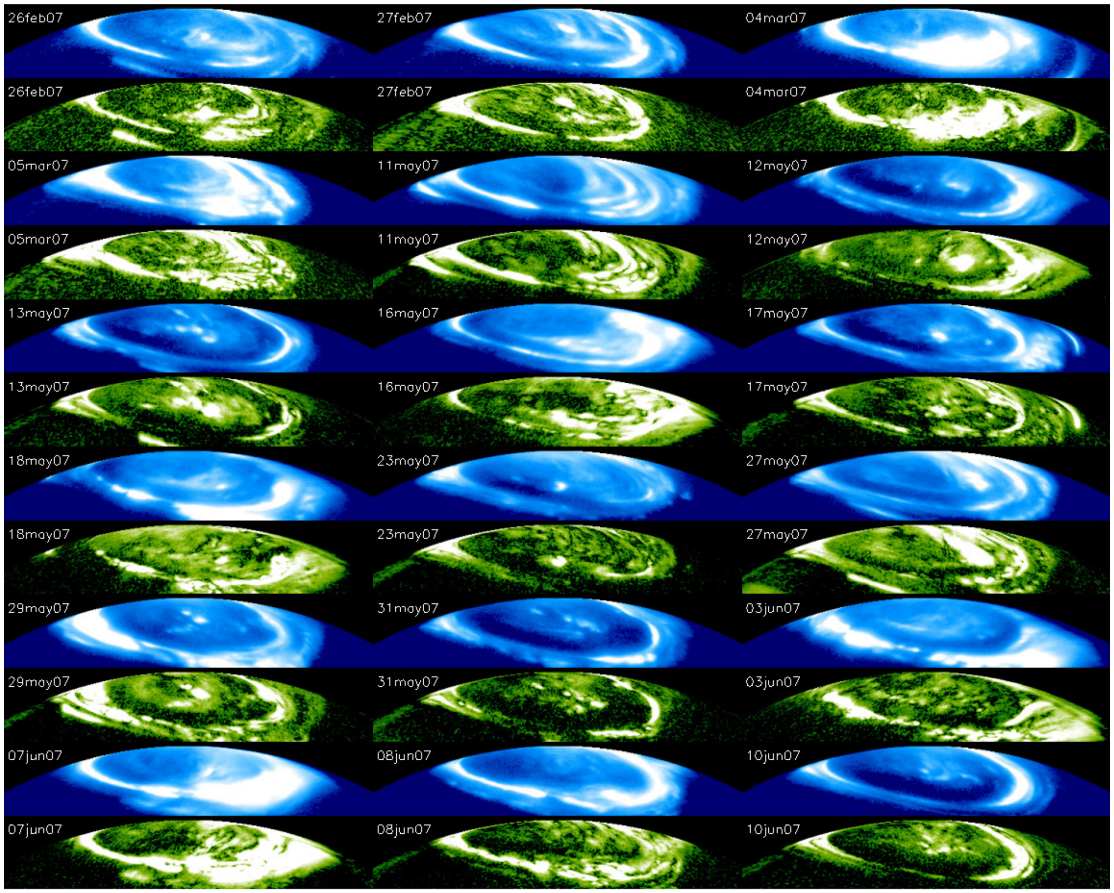

Figure 7: The average auroral emission across each day of observation is shown (blue). For each day, we also show the standard deviations measured within combined images with a time step of 13m 20s (green). These are scaled to a variance of 5 – 80 kR, with a gamma correction of 0.3.

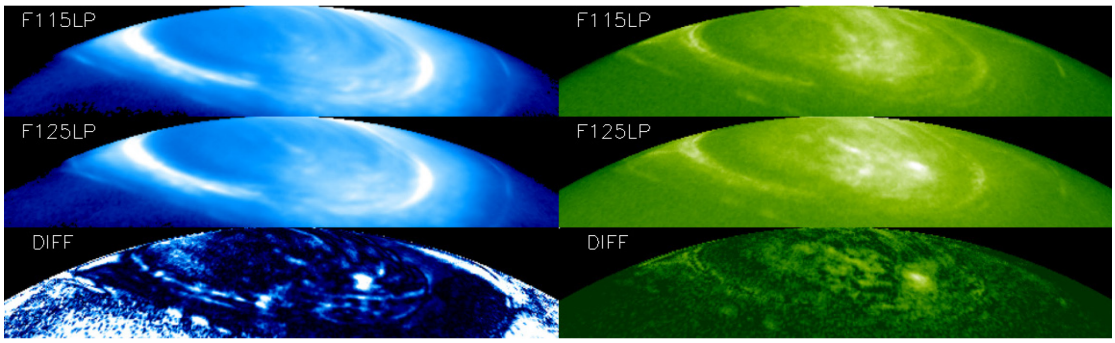

Figure 8: A comparison of the emission and variability observed across this study within the two filters (F115 and F125) used. We show the average emission observed within the two filters (left top and middle), scaled between 2 – 200 kR, with a gamma correction of 0.2. We show the difference between these two images, on a linear scale, scaled to 25% of the average intensity of both filters (left bottom). We also show variability within the two filters by measurement the average difference from image to image for the two filters (right top and middle), scaled between 3 – 60 kR, with a gamma correction of 0.3. We show the difference between these two measurements using the same scaling (bottom right)

Acknowledgements

This work was supported by the UK STFC for H.M., T.S. and J.N., and with a PhD studentship for R.J. Undergraduates. This analysis came about following discussions within the ISSI Team Nichols and Team Stallard workshops. J.E.P. Connerney and Takehiko Satoh were visiting astronomers at the NASA Infrared Telescope Facility, which is operated by the University of Hawaii under Cooperative Agreement no. NNX-08AE38A with the National Aeronautics and Space Administration, Science Mission Directorate, Planetary Astronomy Program. Infrared data is available from

765 the Magnetospheres of the Outer Planets Infrared Data Archive. Ultraviolet data is
766 available from Hubble Legacy Archive.

767 References

768 Achilleos, N., Miller, S., Tennyson, J., Aylward, A. D., Mueller-Wodarg, I., Rees, D.
769 JIM: A time-dependent, three-dimensional model of Jupiter's thermosphere and
770 ionosphere. J. Geophys. Res. 103, 20089-20112. DOI: 10.1029/98JE00947 (1998)

771 Badman, S. V., Branduardi-Raymont, G., Galand, M., Hess, S. L. G., Krupp, N.,
772 Lamy, L., Melin, H., Tao, C. Auroral Processes at the Giant Planets: Energy
773 Deposition, Emission Mechanisms, Morphology and Spectra, Space Science Reviews
774 187, 99-179, DOI:10.1007/s11214-014-0042-x (2015)

775 Bonfond, B., Grodent, D., Gérard, J.-C., Radioti, A., Saur, J., Jacobsen, S. UV Io
776 footprint leading spot: A key feature for understanding the UV Io footprint
777 multiplicity?, Geophysical Research Letters 35, L05107-
778 DOI:10.1029/2007GL032418 (2008)

779 Bonfond, B., Vogt, M. F., Gérard, J.-C., Grodent, D., Radioti, A., Coumans, V.
780 Quasi-periodic polar flares at Jupiter: A signature of pulsed dayside reconnections?
781 Geophysical Research Letters 38, L02104, DOI: 10.1029/2010GL045981 (2011)

782 Bonfond, B.; Grodent, D.; Gérard, J.-C.; Stallard, T.; Clarke, J. T.; Yoneda, M.;
783 Radioti, A.; Gustin, J. Auroral evidence of Io's control over the magnetosphere of
784 Jupiter. Geophysical Research Letters, Volume 39, Issue 1, CiteID L01105, DOI:
785 10.1029/2011GL050253 (2012)

786 Caldwell, J., A. T. Tokunaga, and G. S. Orton, Further observations of 8-□m polar
787 brightenings of Jupiter, *Icarus*, *53*, 133–140, 1983

788 Clarke, John T. and 20 co-authors. Far-Ultraviolet Imaging of Jupiter's Aurora and the
789 lo "Footprint". Science 274, 404-409. DOI: 10.1126/science.274.5286.404 (1996)

790 Clarke, J. T., Ajello, J., Ballester, G., Ben Jaffel, L., Connerney, J., Gérard, J.-C.,
791 Gladstone, G. R., Grodent, D., Pryor, W., Trauger, J., Waite, J. H. Ultraviolet
792 emissions from the magnetic footprints of Io, Ganymede and Europa on Jupiter,
793 Nature 415, 997-1000, (2002)

794 Clarke, John T., Grodent, Denis, Cowley, Stan W. H., Bunce, Emma J., Zarka,
795 Philippe, Connerney, John E. P., Satoh, Takehiko. Jupiter's aurora. In: Jupiter. The
796 planet, satellites and magnetosphere. Edited by Fran Bagenal, Timothy E. Dowling,
797 William B. McKinnon. Cambridge planetary science, Vol. 1, Cambridge, UK:
798 Cambridge University Press, p. 639 – 670. ISBN 0-521-81808-7 (2004)

799 Clarke, J. T. and 20 co-authors. Response of Jupiter's and Saturn's auroral activity to
800 the solar wind. J. Geophys. Res. 114, CiteID A05210. DOI: 10.1029/2008JA013694
801 (2009)

802 Connerney, J. E. P., Baron, R., Satoh, T., Owen, T. Images of Excited H_3^+ at the Foot
803 of the Io Flux Tube in Jupiter's Atmosphere. Science 262, 1035-1038. DOI:
804 10.1126/science.262.5136.1035 (1993)

805 Cowley, S.W.H. and Bunce, E.J. Origin of the main auroral oval in Jupiter's coupled
806 magnetosphere-ionosphere system. Planet. Space Sci. 49, 1067-1088. DOI:
807 10.1016/S0032-0633(00)00167-7 (2001)

808 Cowley, S. W. H., Bunce, E. J., Stallard, T. S., Miller, S. Jupiter's polar ionospheric
809 flows: Theoretical interpretation. Geophys. Res. Lett. 30, 24-1, DOI:
810 10.1029/2002GL016030 (2003)

811 Delamere, P. A., Bagenal, F. J. Solar wind interaction with Jupiter's magnetosphere.
812 Geophys. Res. 115, A10201, DOI: 10.1029/2010JA015347 (2010)

813 Delamere, P. A., Bagenal, F., Paranicas, C., Masters, A., Radioti, A., Bonfond, B.,
814 Ray, L., Jia, X., Nichols, J., Arridge, C.. Solar Wind and Internally Driven Dynamics:
815 Influences on Magnetodiscs and Auroral Responses, Space Science Reviews 187,
816 51-97, DOI:10.1007/s11214-014-0075-1 (2015)

817 Grodent, D., Clarke, J. T., Waite, J. H., Cowley, S. W. H., GéRard, J.-C., Kim, J.
818 Jupiter's polar auroral emissions. J. Geophys. Res. 108, SMP 6-1, CiteID 1366, DOI
819 10.1029/2003JA010017 (2003a)

820 Grodent, D., Clarke, J. T., Kim, J., Waite, J. H., Cowley, S. W. H. Jupiter's main
821 auroral oval observed with HST-STIS, Journal of Geophysical Research (Space
822 Physics) 108, 1389- DOI:10.1029/2003JA009921 (2003b)

823 Grodent, Denis, Bonfond, Bertrand, GéRard, Jean-Claude, Radioti, Aikaterini, Gustin,
824 Jacques, Clarke, John T., Nichols, Jonathan, Connerney, John E. P. Auroral evidence
825 of a localized magnetic anomaly in Jupiter's northern hemisphere J. Geophys. Res.
826 113, A09201. DOI: 10.1029/2008JA013185 (2008)

827 Grodent, D. A Brief Review of Ultraviolet Auroral Emissions on Giant Planets,
828 Space Science Reviews 187, 23-50, DOI:10.1007/s11214-014-0052-8 (2015)

829 Hess, S. L. G., Bonfond, B., Zarka, P., Grodent, D. Model of the Jovian magnetic
830 field topology constrained by the Io auroral emissions. Journal of Geophysical
831 Research, 116, A05217, DOI: 10.1029/2010JA016262 (2011)

832 Kim, S.J., Caldwell, J., Rivolo, A.R., Wagener, R., Orton, G.S., 1985. Infrared polar
833 brightening on Jupiter. III. Spectrometry from the Voyager 1 IRIS experiment. Icarus
834 64, 233–248.
835
836 Kimura, T., Badman, S. V., Tao, C., Yoshioka, K., Murakami, G., Yamazaki, A.,
837 Tsuchiya, F., Bonfond, B., Steffl, A. J., Masters, A., Kasahara, S., Hasegawa, H.,
838 Yoshikawa, I., Fujimoto, M., Clarke, J. T.. Transient internally driven aurora at
839 Jupiter discovered by Hisaki and the Hubble Space Telescope, Geophysical Research
840 Letters 42, 1662-1668, DOI:10.1002/2015GL063272 (2015)

841 Melin, Henrik, Miller, Steve, Stallard, Tom, Smith, Chris, Grodent, Denis. Estimated
842 energy balance in the jovian upper atmosphere during an auroral heating event. Icarus
843 181, 256-265, DOI: 10.1016/j.icarus.2005.11.004 (2006)

844 Nichols, J. D.; Clarke, J. T.; Gérard, J. C.; Grodent, D. Observations of Jovian polar
845 auroral filaments. Geophysical Research Letters 36, L08101, DOI:
846 10.1029/2009GL037578 (2009a)

847 Nichols, J. D., Clarke, J. T., Gérard, J. C., Grodent, D., Hansen, K. C.
848 Variation of different components of Jupiter's auroral emission, Journal of
849 Geophysical Research (Space Physics) 114, A06210- DOI:10.1029/2009JA014051
850 (2009b)

851 Pallier, L., Prangé, R. More about the structure of the high latitude Jovian aurorae.
852 Planetary and Space Science 49, 1159-1173. DOI: 10.1016/S0032-0633(01)00023-X
853 (2001)

854 Radioti, A., Lystrup, M., Bonfond, B., Grodent, D., Gérard, J.-C., Jupiter's aurora in
855 ultraviolet and infrared: Simultaneous observations with the Hubble Space Telescope
856 and the NASA Infrared Telescope Facility. J. Geophys. Res. 118, 2286-2295, DOI:
857 10.1002/jgra.50245 (2013)

858 Raynaud, E., Lellouch, E., Maillard, J.-P., Gladstone, G. R., Waite, J. H., Bézard, B.,
859 Drossart, P., Fouchet, T. Spectro-imaging observations of Jupiter's 2-μm auroral
860 emission. I. H_3^+ distribution and temperature, Icarus 171, 133-152,
861 DOI:10.1016/j.icarus.2004.04.020 (2004)

862 Satoh, Takehiko, Connerney, J. E. P. Jupiter's H_3^+ Emissions Viewed in Corrected
863 Jovimagnetic Coordinates. Icarus 141, 236-252. DOI: 10.1006/icar.1999.6173 (1999)

864 Shure, Mark A., Toomey, Douglas W., Rayner, John T., Onaka, Peter M., Denault,
865 Anthony J. NSFCAM: a new infrared array camera for the NASA Infrared Telescope
866 Facility. Proc. SPIE 2198, 614-622, (1994)

867 Stallard, Tom, Miller, Steve, Millward, George, Joseph, Robert D. On the Dynamics
868 of the Jovian Ionosphere and Thermosphere: I. The Measurement of Ion Winds.
869 Icarus 154, 475-491, DOI: 10.1006/icar.2001.6681 (2001)

870 Stallard, T. S., Miller, S., Cowley, S. W. H., Bunce, E. J. Jupiter's polar ionospheric
871 flows: Measured intensity and velocity variations poleward of the main auroral oval.
872 Geophysical Research Letters 30, 25-1, DOI 10.1029/2002GL016031 (2003)

873 Stallard Tom S., Henrik Melin, Steve Miller, Sarah V. Badman, Kevin H. Baines,
874 Robert H. Brown, James S. D. Blake, James O'Donoghue, Rosie E. Johnson, Bethany
875 Bools, Nathan M. Pilkington, Oliver T.L. East, and Mark Fletcher. Cassini VIMS
876 observations of H3+ emission on the nightside of Jupiter. Journal of Geophysical
877 Research (Space Physics), in press. (2015)

878 Tao, Chihiro, Badman, Sarah V., Fujimoto, Masaki. UV and IR auroral emission
879 model for the outer planets: Jupiter and Saturn comparison. Icarus 213, 581-592, DOI:
880 10.1016/j.icarus.2011.04.001 (2011)

881 Trafton, L., Carr, J., Lester, D., Harvey, P.. A possible detection of Jupiter's northern
882 auroral S1(1) H2 quadrupole line emission, Icarus 74, 351-356, DOI:10.1016/0019-
883 1035(88)90047-4 (1988)

884 Vogt, M. F., Kivelson, M. G., Khurana, K. K., Walker, R. J., Bonfond, B., Grodent,
885 D., Radioti, A. Improved mapping of Jupiter's auroral features to magnetospheric
886 sources, Journal of Geophysical Research (Space Physics) 116, A03220-
887 DOI:10.1029/2010JA016148 (2011)